

# A systematic study of neutron magic nuclei with $N = 8, 20, 28, 50, 82$ , and $126$ in the relativistic mean field theory

L. S. Geng,<sup>1,2</sup> H. Toki,<sup>1</sup> and J. Meng<sup>2</sup>

<sup>1</sup>*Research Center for Nuclear Physics (RCNP), Osaka University, Ibaraki, Osaka 567-0047, Japan*

<sup>2</sup>*School of Physics, Peking University, Beijing 100871, People's Republic of China*

We perform a systematic study of all the traditional neutron magic nuclei with  $N = 8, 20, 28, 50, 82$ , and  $126$ , from the neutron drip line to the proton drip line. We adopt the deformed relativistic mean field (RMF) theory as our framework and treat pairing correlations by a simple BCS method with a zero-range  $\delta$ -force. Remarkable agreement with the available experimental data is obtained for the binding energies, the two- and one-proton separation energies, and the nuclear charge radii. The calculated nuclear deformations are compared with the available experimental data and the predictions of the FRDM mass formula and the HFBCS-1 mass formula. We discuss, in particular, the appearance of sub-shell magic nuclei by observing irregular behavior in the two- and one-proton separation energies.

## I. INTRODUCTION

“Magic number” is a very important concept in many subjects of physics, such as atomic physics, nuclear physics and micro cluster physics. In nuclear physics, nuclei with magic numbers have been hot topics of nuclear research since the beginning of this subject [1, 2]. In recent experiments with radioactive nuclear beams (RNB), disappearance of traditional magic numbers and appearance of new magic numbers are observed in nuclei with exotic isospin ratios. Furthermore, nuclei with magic neutron numbers in the neutron-rich region are of special interest for the study of astrophysical r-process [3].

The unusual stability of nuclei with neutron (proton) numbers 2, 8, 20, 28, 50, 82, and 126, commonly referred to as “magic numbers”, was traditionally explained in the nonrelativistic shell model approximated by the 3D Harmonic-Oscillator central potential together with a very strong spin-orbit interaction introduced by hand [1, 2, 4, 5, 6]. On the other hand, in the models within the relativistic framework, say the relativistic mean field (RMF) theory [7, 8, 9, 10, 11], the strong spin-orbit interaction appears naturally as the interplay between the strong scalar and vector potentials, which are necessary for reproducing the saturation properties of nuclear matter. Due to the proper setting of the scalar and the vector potentials the shell structure is obtained without any additional parameters for the spin-orbit splittings.

Recently, it is argued that the magic numbers are of a localized feature, i.e. in nuclei with exotic isospin ratios the classical magic numbers do not necessarily hold and new magic numbers may appear. There have been several experimental evidences supporting such a belief, including the lately reported  $N = 82$  shell quenching [12] and the appearance of a new neutron magic number  $N = 16$  in the neutron-rich light nuclei [13]. Such a localized feature of magic numbers are also claimed to be important for various nuclear-astrophysical problems [14]. The disappearance or quenching of nuclear magicity near both neutron and proton drip lines have been discussed quite a lot in various nuclear models, includ-

ing the infinite nuclear matter (INM) model [15], the extended Bethe-Weizsäcker mass formula [16], the antisymmetrized molecular dynamics (AMD) [17], the Hartree-Fock method [18], and the relativistic mean field (RMF) [19, 20] theory. In the relativistic mean field model, while the  $Z = 8, 20, 28, 50, 82$ , and  $126$  isotopic chains have been discussed a lot, a systematic study of all the nuclei with neutron magic numbers is still missing.

The appearance and disappearance of the magic number effect are intimately related with the spin-orbit interaction and the onset of deformation. In this sense, a systematic study of nuclei in various mass regions in terms of the relativistic mean field theory is suited, since the spin-orbit interaction arises naturally in relation with the saturation property. Hence, we are able to provide the variation of the spin-orbit splittings with the proton and neutron numbers. As for the deformation, nuclei with magic numbers are not easy to acquire deformation, because the onset of deformation does not utilize the energy gain coming from the large shell gaps. At the same time, due to this reason it is easier to find the appearance of the sub-magic effects for nuclei with either the proton number or the neutron number being magic numbers.

In the present work, we would like to make a systematic study of neutron magic nuclei from the neutron drip line to the proton drip line in terms of the deformed relativistic mean field theory. The pairing correlations are also very important to make the nucleus tend to be spherical. Therefore, we take the recently proposed method of using the zero-range  $\delta$ -force for the pairing correlations in order to pick up the resonant states in the continuum when the nucleus approaches the neutron threshold [21]. The quadrupole constrained RMF calculation is performed for each nucleus to find all the energy minima as a function of the nuclear deformation. In this paper, we stay our calculations at the mean-field level and hence anticipate that we may miss the onset of small deformation in this framework for the case, in which the deformation effect is not dominant. Hence, the purpose of this paper is to make a systematic study of the neutron magic nuclei in the mean field framework and compare with the avail-

able experimental data in the global sense and with other more sophisticated theoretical models for particular nuclei. We mention that even at the mean-field level, many proton magic nuclei appear to be deformed [20].

This paper is organized as follows. We provide a short summary of the deformed RMF+BCS method in Sec. II. In Sec. III-VI, we present the results of our calculations, including the binding energies, the two- and one-proton separation energies, the nuclear radii, and the nuclear deformations. With these quantities, we also discuss the magicity of these neutron magic nuclei with  $N = 8, 20, 28, 50, 82$ , and  $126$ . The whole work is summarized in Sec. VII.

## II. THEORETICAL FRAMEWORK

In the present work, the recently proposed deformed RMF+BCS method with a zero-range  $\delta$ -force in the pairing channel is adopted [21]. The zero-range  $\delta$ -force has proved to be very successful to take into account the continuum effect by picking up the resonant states both in relativistic and nonrelativistic self-consistent mean field models [21, 22, 23, 24, 25, 26]. In the mean-field part, the TMA parameter set is used [27]. The RMF calculations have been carried out using the model Lagrangian density with nonlinear terms for both  $\sigma$  and  $\omega$  mesons as described in detail in Refs. [21, 27], which is given by

$$\begin{aligned} \mathcal{L} = & \bar{\psi}(i\gamma^\mu\partial_\mu - M)\psi \\ & + \frac{1}{2}\partial_\mu\sigma\partial^\mu\sigma - \frac{1}{2}m_\sigma^2\sigma^2 - \frac{1}{3}g_2\sigma^3 - \frac{1}{4}g_3\sigma^4 - g_\sigma\bar{\psi}\sigma\psi \\ & - \frac{1}{4}\Omega_{\mu\nu}\Omega^{\mu\nu} + \frac{1}{2}m_\omega^2\omega_\mu\omega^\mu + \frac{1}{4}g_4(\omega_\mu\omega^\mu)^2 - g_\omega\bar{\psi}\gamma^\mu\psi\omega_\mu \\ & - \frac{1}{4}R_{\mu\nu}^aR^{a\mu\nu} + \frac{1}{2}m_\rho^2\rho_\mu^a\rho^{a\mu} - g_\rho\bar{\psi}\gamma_\mu\tau^a\psi\rho^{a\mu} \\ & - \frac{1}{4}F_{\mu\nu}F^{\mu\nu} - e\bar{\psi}\gamma_\mu\frac{1-\tau_3}{2}A^\mu\psi, \end{aligned} \quad (1)$$

where all symbols have their usual meanings. The corresponding Dirac equations for nucleons and Klein-Gordon equations for mesons obtained with the mean-field approximation are solved by the expansion method on the widely used axially deformed Harmonic-Oscillator basis [21, 28]. The number of shells used for expansion is chosen as  $N_f = N_b = 20$ . More shells have been tested for convergence considerations. The quadrupole constrained calculations have been performed for all the nuclei considered here in order to obtain their potential energy surfaces (PESs) and determine the corresponding ground-state deformations [21, 29]. For nuclei with odd number of nucleons, a simple blocking method without breaking the time-reversal symmetry is adopted [5, 30]. The pairing strength  $V_0$  is taken to be the same for both protons and neutrons, but optimized for different regions by fitting the experimental two- and one-proton separation energies, more specifically, for the  $N = 8, 20, 28, 50$  isotonic chains,  $V_0 = 344.1$  MeV fm $^3$ ; for the  $N = 82, 126$  isotonic chains,  $V_0 = 310$  MeV fm $^3$ .

Whenever the zero-range  $\delta$  force is used either in the BCS or the Bogoliubov framework, a cutoff procedure must be applied, i.e. the space of the single-particle states where the pairing interaction is active must be truncated. This is not only to simplify the numerical calculation but also to simulate the finite-range (more precisely, long-range) nature of the pairing interaction in a phenomenological way [31, 32]. In the present work, the single-particle states subject to the pairing interaction are confined to the region satisfying

$$\epsilon_i - \lambda \leq E_{\text{cut}}, \quad (2)$$

where  $\epsilon_i$  is the single-particle energy,  $\lambda$  the Fermi energy, and  $E_{\text{cut}} = 8.0$  MeV. We find that increasing  $E_{\text{cut}}$  from 8.0 MeV up to 16.0 MeV, followed by a readjustment of the pairing strength  $V_0$ , does not change the results appreciably, and therefore none of our conclusions will change. Recently, such a cutoff issue has been discussed in much detail by Goriely et al. in the Hartree-Fock-Bogoliubov (HFB) framework [32]. Our cutoff procedure happens to coincide with their conclusions (see Table II of Ref. [32]), although a bit different from their final optimal choice used in the construction of the HFB-2 mass table.

Even after the pairing interaction between like nucleons is taken into account, mean-field calculations (HF or RMF) still miss some residual correlations, one of which is the so-called Wigner effect. Such an effect is known to be important for light  $N \approx Z$  nuclei by making them more bound by about 2 MeV. Although it is usually approximated in a phenomenological way in most mass tables [32, 33, 34, 35, 36], here we will ignore this effect due to the following considerations. It is expected that these residual correlations (including the Wigner effect) have only small contributions and are active only under special situations. In the case of the Wigner effect, it becomes appreciable only for light nuclei with  $N \approx Z$ .

Finally, the center-of-mass correction is approximated by

$$E_{\text{cm}} = -\frac{3}{4}41A^{-1/3}, \quad (3)$$

which is often used in the relativistic mean field theory among the many recipes for the center-of-mass correction [37]. Since adopting new schemes implies that one has to readjust the model parameters, we will adhere to this simple approximation in the present work.

## III. BINDING ENERGIES

The nuclear binding energy is one of the most basic properties of nuclei. Although the two- and one-proton separation energies are more useful for the purpose of identifying the shell structure, the binding energies of nuclei can also show some important features of a theoretical model, such as the reliability of the extrapolation

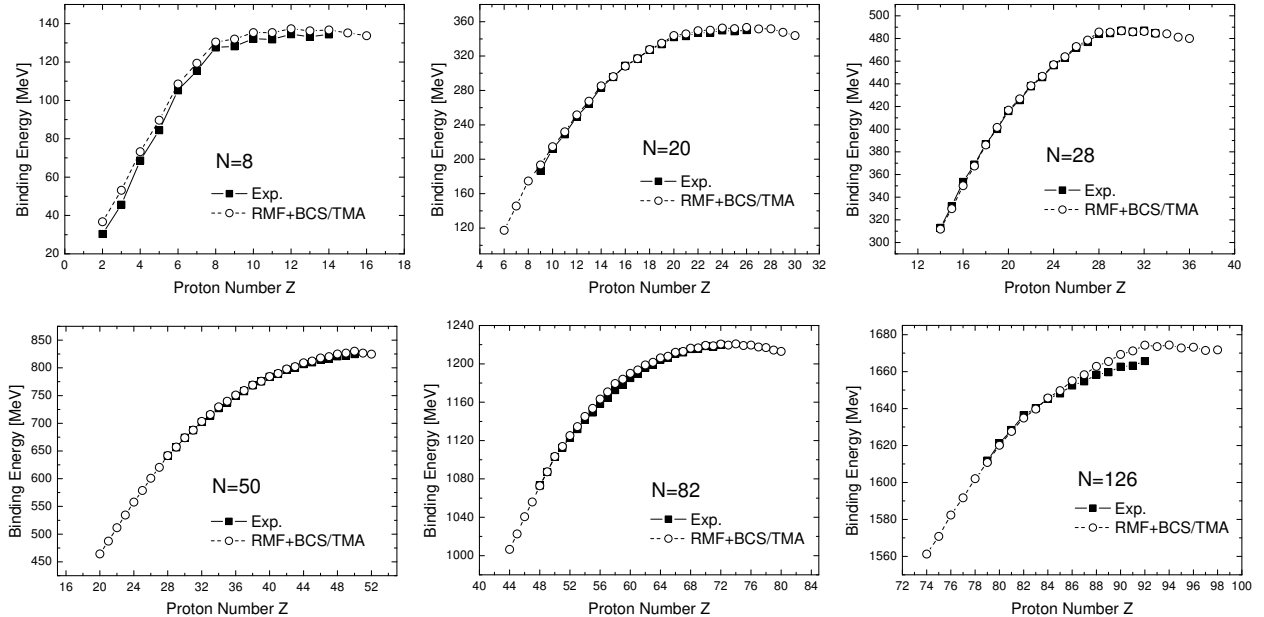


FIG. 1: The binding energies of the  $N = 8, 20, 28, 50, 82$ , and  $126$  isotones as functions of the proton number,  $Z$ . The results obtained from the deformed RMF+BCS calculations with the TMA parameter set (open circle) are compared with the available experimental data (solid square) [38].

to the unknown areas. In Fig. 1, we compare the binding energies of all the isotones with neutron number  $N = 8, 20, 28, 50, 82$ , and  $126$  with the available experimental data [38]. Remarkable agreement between theory and experiment can be clearly seen. For the  $N = 8$  isotonic chain, the experimental trend is reproduced quite well. The only small discrepancy is that the calculated results are somewhat systematically larger than the experimental data. Nevertheless, it is surprising that a mean field model can reproduce such light nuclei so well without fitting the parameters particularly for this region. For the  $N = 126$  isotonic chain, theory agrees well with experiment around  $^{208}\text{Pb}$ . The results for nuclei with more protons begin to deviate from the experimental data, i.e. the calculated results are larger than the experimental data. The use of other parameter sets, NL3 [39] and NL-Z2 [40], does not change this conclusion.

It is well known that the modern HF or RMF calculations still can not provide a description of nuclear masses comparable to those of most mass tables [41]. This feature is attributed to the limited number of nuclear masses taken into account in the fitting procedure of the model parameters. On the other hand, when more masses are included into the fitting procedure as what has been done by Goriely et al. [32, 33, 34, 35], a description of nuclear masses comparable to that of the finite-range droplet model (FRDM) [36] has been obtained based on the HF [33] and HFB [32, 34, 35] methods. In Table I, we compare the root-mean-square (rms) deviation  $\sigma$  of our present calculation, with that of the HFBCS-1 mass formula, and that of the FRDM model for 107 nuclei whose

experimental (or extrapolated) masses are compiled in Ref. [38].

TABLE I: The mass rms deviation  $\sigma$  for 107 nuclei with  $N = 8, 20, 28, 50, 82$ , and  $126$  from the present calculation (RMF+BCS), the HFBCS-1 mass formula (HFBCS-1) [33], and the FRDM mass formula (FRDM) [36].

	RMF+BCS	HFBCS-1[33]	FRDM[36]
$\sigma$	2.873	0.957	0.774

It is easily seen that the rms deviation of the present RMF calculation is still 3 times larger than that of the HFBCS-1 mass formula or 4 times larger than that of the FRDM model. It should be noted that the rms deviations for the HFBCS-1 mass formula and for the FRDM mass formula shown in Table I are larger than their overall deviations, 0.738 MeV and 0.669 MeV, respectively, mainly due to the relatively large discrepancies for those light isotones with  $N = 8, 20$ , and  $28$ . It is expected that a better description of nuclear masses in the RMF framework be obtained if more masses are taken into account in the parameter fitting procedure.

#### IV. TWO- AND ONE-PROTON SEPARATION ENERGIES

The two- and one-proton separation energies

$$S_{2p}(N, Z) = B(N, Z) - B(N, Z - 2), \quad (4)$$

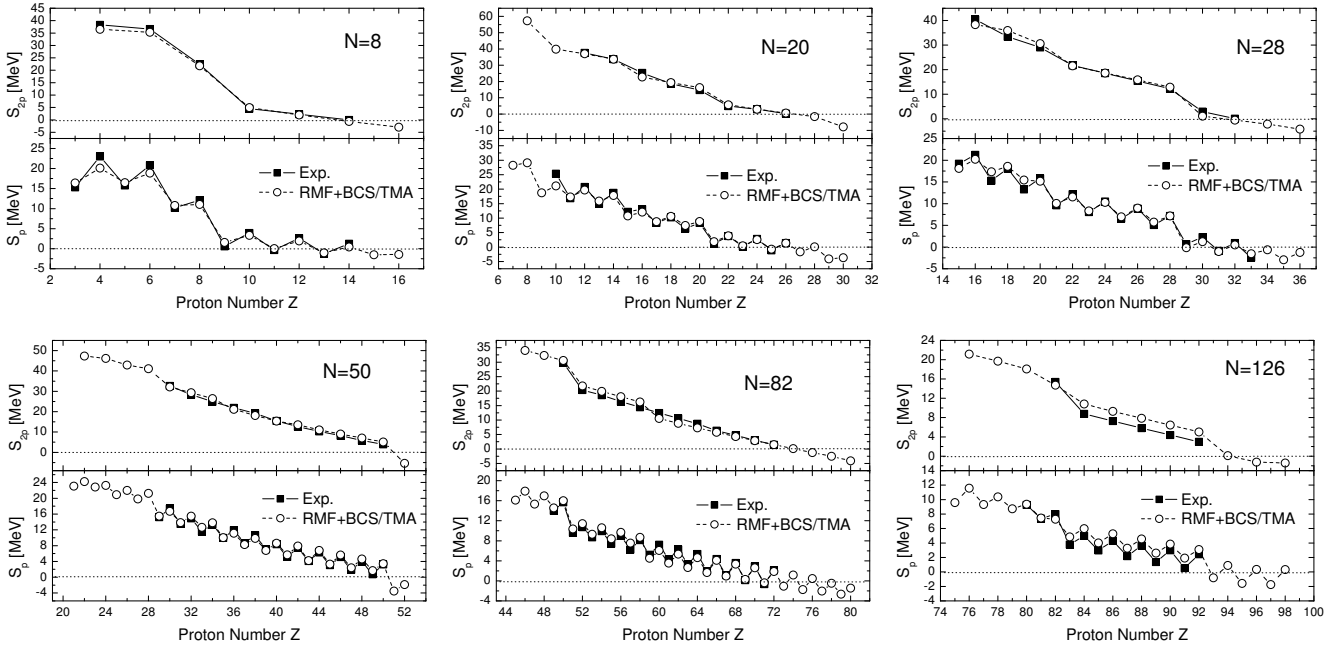


FIG. 2: The two- and one-proton separation energies,  $S_{2p}$  and  $S_p$ , of the  $N = 8, 20, 28, 50, 82$ , and  $126$  isotones as functions of the proton number,  $Z$ . The results obtained from the deformed RMF+BCS calculations with the TMA parameter set (open circle) are compared with the available experimental data (solid square) [38].

$$S_p(N, Z) = B(N, Z) - B(N, Z - 1), \quad (5)$$

where  $B(N, Z)$  is the binding energy of the nucleus with neutron number  $N$  and proton number  $Z$ , are quite important and sensitive quantities to describe nuclei and the corresponding shell closures. In Fig. 2, we plot the two- and one-proton separation energies for all the  $N = 8, 20, 28, 50, 82$ , and  $126$  isotones as functions of the proton number  $Z$ . A larger drop than its neighboring counterparts in these curves is usually interpreted as a (sub)shell closure, and the corresponding nucleon number is called “(sub-)magic number”. In the present work, we mainly adopt such a notion to discuss shell closures.

In Fig. 2, the calculated two- and one-proton separation energies are compared with the available experimental data [38]. We should mention that some experimental data from Ref. [38] are obtained by “distant connection” and that we do not make any distinction between real experimental data and extrapolated data. From Fig. 2, it is quite clear that the theoretical calculations agree remarkably well with the experimental data in the whole region from mass number  $11$  ( $^{11}\text{Li}_8$ ) to mass number  $218$  ( $^{218}\text{U}_{126}$ ).

For the  $N = 8$  isotonic chain, the  $Z = 8$  ( $1p_{1/2}$ ) shell closure is clearly seen from both the two- and the one-neutron separation energies, where the shell quantum number in the bracket is that of the shell closure. Both experimental data and our calculations also show a distinct shell closure at  $Z = 6$  ( $1p_{3/2}$ ). For the  $N = 20$  isotonic chain, in addition to the traditional  $Z = 8$  ( $1p_{1/2}$ ),  $Z = 20$  ( $1d_{3/2}$ ), and  $Z = 28$  ( $1f_{7/2}$ ) shell closures, a

new (sub)shell closure ( $1d_{5/2}$ ) is clearly seen at  $Z = 14$ .  $^{34}\text{Si}_{20}$  has been recognized as a doubly magic nucleus by a previous shell-model calculation [42], due to a feature characteristic of doubly magic nuclei, i.e. it has a  $0p - 0h$  ground state and its two lowest excited states are intruders. For the  $N = 28$  isotonic chain, two neutron shell closures at  $Z = 20$  ( $1d_{3/2}$ ) and  $Z = 28$  ( $1f_{7/2}$ ) are reproduced quite well. For the  $N = 50$  isotonic chain, the agreement with the available experimental data is very good. Although the  $Z = 28$  ( $1f_{7/2}$ ) and  $Z = 50$  ( $1g_{9/2}$ ) shell closures are still unaccessible experimentally up to now, they are clearly shown in our calculations. Based on the overall good agreement of the  $N = 50$  isotonic chain, we believe that our predictions are reliable.

For the  $N = 82$  isotonic chain, the  $Z = 50$  ( $1g_{9/2}$ ) shell closure is reproduced quite well while the  $Z = 82$  ( $1h_{11/2}$ ) shell closure is already in the unbound region. We note that there is a new (sub)shell closure at  $Z = 58$  ( $1g_{7/2}$ ), as shown in Fig. 2. It was argued long time ago that there is a whole “plateau” of stability for all the even  $58 \leq Z \leq 70$  nuclei in the  $N = 82$  isotonic chain [43, 44], i.e. the so-called “changing magicities”. Our calculations do indicate this (sub)shell closure, which is also supported by the experimental data, as shown in Fig. 2. However, the different deviation trends for nuclei with  $Z > 58$  and  $Z < 58$  indicate that some important features around  $Z = 58$  in the  $N = 82$  isotonic chain may be missed and/or mistreated in the relativistic mean field theory.

For the  $N = 126$  isotonic chain, immediately, we notice the seemingly big deviations of our calculations from

the experimental data. From both the two- and the one-proton separation energies, we note that the experimental  $Z = 82$  ( $1h_{11/2}$ ) shell closure is underestimated somewhat by the relativistic mean field calculations. Our calculations also indicate another new (sub)shell closure ( $1h_{9/2}$ ) at  $Z = 92$  in agreement with Ref. [45], where  $^{218}_{92}\text{U}_{126}$  is studied as a doubly magic nucleus. We notice that this is a unique phenomenon in the relativistic mean field theory while a large-scale shell-model calculation did not find this shell closure [46]. We also find that the use of other often used parameter sets in this region, such as NL3 [39] and NL-Z2 [40], does not change our conclusion.

The two-proton separation energy becomes negative when the nucleus becomes unstable with respect to two-proton emission. Hence, the two-proton drip-line nucleus for the corresponding isotonic chain is the one with two less protons than the nucleus at which  $S_{2p}$  first becomes negative. In the same way, we can also name the one-proton drip-line nucleus. The predicted two- and one-proton drip-line nuclei based on our calculations are  $^{20}_{12}\text{Mg}_8$ ;  $^{46}_{26}\text{Fe}_{20}$ ,  $^{44}_{24}\text{Cr}_{20}$ ;  $^{58}_{30}\text{Zn}_{28}$ ,  $^{56}_{28}\text{Ni}_{28}$ ;  $^{100}_{50}\text{Sn}_{50}$ ;  $^{156}_{74}\text{W}_{82}$ ,  $^{152}_{70}\text{Yb}_{82}$ ;  $^{220}_{94}\text{Pu}_{126}$ ;  $^{218}_{92}\text{U}_{126}$ ; respectively. It is interesting to note that in some cases the two-proton drip-line nucleus and the one-proton drip-line nucleus are the same one, such as  $^{20}_{12}\text{Mg}_8$  in the  $N = 8$  isotonic chain and  $^{100}_{50}\text{Sn}_{50}$  in the  $N = 50$  isotonic chain. In other cases, the one-proton drip-line nucleus comes before the two-proton drip-line nucleus, which is easy to understand because the pairing interaction can increase the stability of even-even nuclei compared with its one-neutron less isotope. Depending on the pairing strength of the specific situation, the difference in neutron number between the two- and one-proton drip-line nucleus could be two or four. More specifically, the difference is 2 in the  $N = 20$ , 28 and 126 isotonic chains, while it is 4 in the  $N = 82$  isotonic chain.

## V. NUCLEAR RADII

The difference between neutron and proton root-mean-square (rms) radii,

$$R_{n(p)} = \langle r_{n(p)}^2 \rangle^{1/2} = \left[ \frac{\int \rho_{n(p)} r^2 d\mathbf{r}}{\int \rho_{n(p)} d\mathbf{r}} \right]^{1/2}, \quad (6)$$

where  $\rho_{n(p)}$  is the neutron (proton) density distribution, can be very large for nuclei with exotic isospin ratios, thus forms the so-called neutron (proton) skin [30], and even neutron (proton) halo [23, 24, 25]. The neutron rms radii (empty square) and proton rms radii (empty circle) of the  $N = 8, 20, 28, 50, 82$  and 126 isotones are plotted in Fig. 3, where the experimental proton radii (solid circle with error bar) are extracted from the experimental charge radii [47] by the formula,

$$R_p^2 = R_c^2 - 0.64 \text{ fm}^2. \quad (7)$$

Since the HFBCS-1 mass formula has achieved an unprecedented success in describing nuclear charge radii [48] compared with the compilation of Nadjakov et al. [49], its results are also shown for comparison (open stars).

In Fig. 3, it is clearly seen that the agreement between our calculations and the experimental data is remarkably good. For  $^{37}_{17}\text{Cl}_{20}$  and  $^{50}_{22}\text{Ti}_{28}$ , the experimental data are somewhat larger than our theoretical predictions. Also, the proton radii of two nuclei in the  $N = 126$  isotonic chain,  $^{208}_{82}\text{Pb}_{126}$  and  $^{209}_{83}\text{Bi}_{126}$ , seem to be overestimated a bit in our calculations. Some kinks in Fig. 3 are due to the sudden changes of deformations of the corresponding nuclei (see Fig. 4), including the one at  $Z = 16$  in the  $N = 28$  isotonic chain, the one at  $Z = 25$  in the  $N = 50$  isotonic chain, and the one at  $Z = 97$  in the  $N = 126$  isotonic chain. It should be noted that the last few nuclei in each isotonic chain shown in Fig. 3 are unbound in our calculations with separation energies  $-5 < S_{p(2p)} < 0$  MeV (see Fig. 2), thus the sudden increases of the proton radii do not necessarily imply appearances of proton halos.

The agreement between our results and those of the HFBCS-1 [33] mass formula is also very good in general, particularly for those nuclei in the  $N = 50$  and 82 isotonic chains. The discrepancies for some nuclei with  $Z \approx 12$  in the  $N = 20$  isotonic chain are due to the deformation effects (see Fig. 4). And the same is true for the nuclei with  $17 \leq Z \leq 30$  in the  $N = 28$  isotonic chain, but the experimental data seems to be in favor of our results. For all the nuclei in the  $N = 126$  isotonic chain, the results of the HFBCS-1 mass formula are a bit smaller than our results and therefore are closer to the experimental data.

One more thing we note is that unlike proton radii, which go up almost monotonously with increasing proton number, neutron radii usually go down first, then go up slowly. This phenomenon is more obvious in the  $N = 8, 20, 28$ , and 50 isotonic chains. The underlying reason is not difficult to understand. For proton-deficient nuclei with small  $Z$ , the protons occupy “inner” single-particle states with much smaller rms radius than the neutron rms radius. Therefore, an extra proton added to these “inner” single-particle states attracts the neutrons closer to the nuclear center. Consequently, the neutron rms radius decreases until Pauli principle prohibits further protons from occupying these “inner” single-particle states. With more protons added, the opposite becomes true and the neutron rms radius begins to increase, though very slowly.

## VI. DEFORMATIONS

Deformation is another important property of nuclei. It also could be used as one of the indicators of magicity conserving or losing of the corresponding nucleus. In our previous work [20], we found that Sn isotopes are deformed in the neutron-rich region, which could be viewed as the magicity losing of proton magic number  $Z = 50$ .

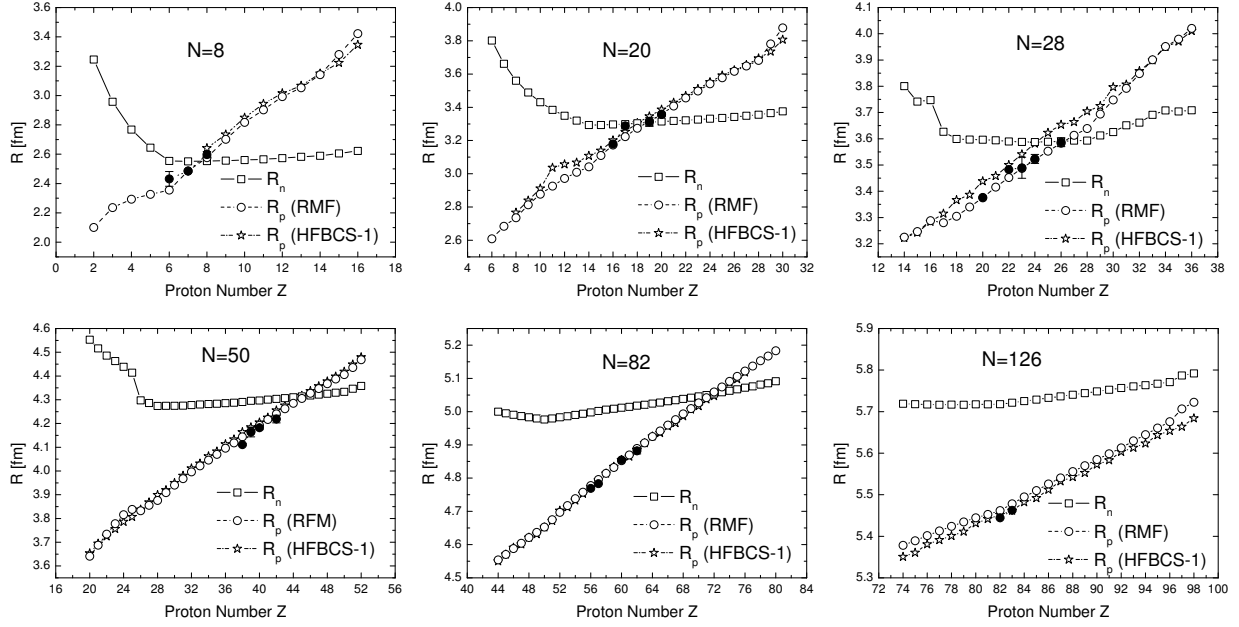


FIG. 3: The rms neutron and proton radii,  $R_n$  and  $R_p$ , of the  $N = 8, 20, 28, 50, 82$ , and  $126$  isotones as functions of the proton number,  $Z$ . The results obtained from the deformed RMF+BCS calculations with the TMA parameter set (open circle) are compared with the available experimental data (solid circle with error bar) [47] and those of the HFBCS-1 mass formula (open star) [33].

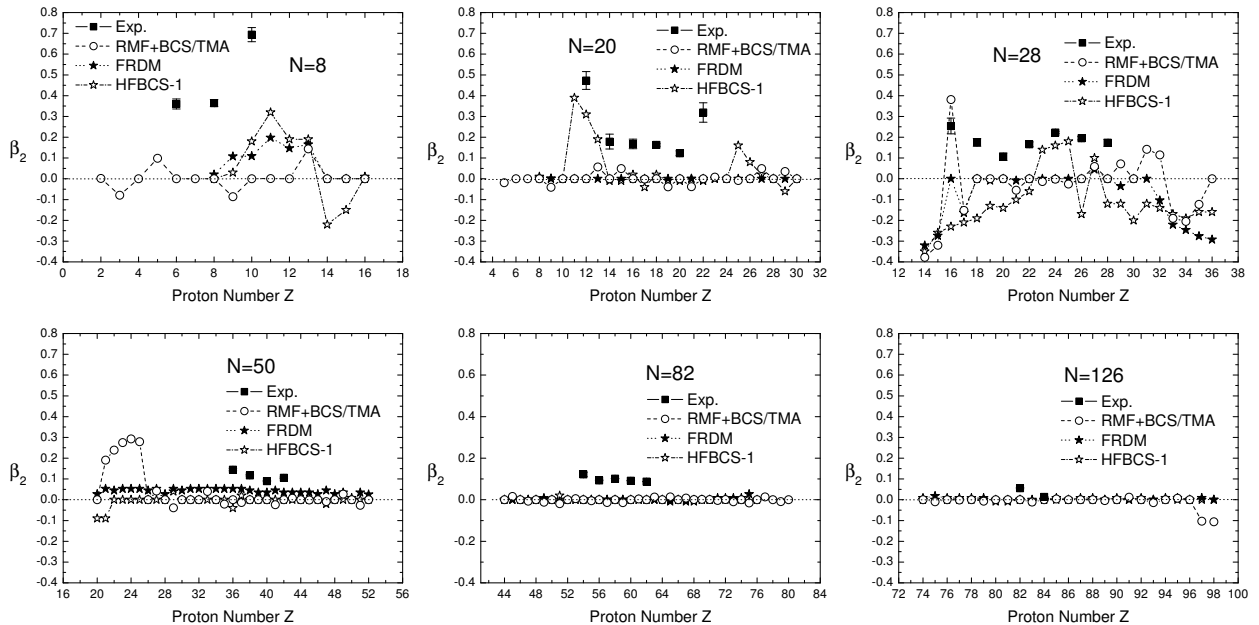


FIG. 4: The mass quadrupole deformation parameters,  $\beta_2$ , of the  $N = 8, 20, 28, 50, 82$ , and  $126$  isotones as functions of the proton number,  $Z$ . The results obtained from the deformed RMF+BCS calculations with the TMA parameter set (open circle) are compared with the predictions of the FRDM model (solid star) [36], those of the HFBCS-1 mass formula (open star) [33], and the available experimental data (solid square with error bar) extracted from the  $B(E2 : 0^+ \rightarrow 2^+)$  values [51]. Note that the extracted deformation parameter does not mean that the corresponding nucleus is really deformed.

However, experimentally, it is difficult to obtain deformation knowledge of nuclei directly. One of the most usual methods is to extract deformation parameters  $\beta_2$  from the  $B(E2 : 0^+ \rightarrow 2^+)$  values by using the assumption of deformation [51]. Hence, all the nuclei have a finite deformation and also the analysis is limited to even-even nuclei. Due to this fact, we have to treat the extracted deformation parameters with care. For most cases, if the extracted deformation parameter is small, the nucleus is expected to be spherical.

In Fig. 4, we plot the mass deformation parameters,  $\beta_2$ , for all the  $N = 8, 20, 28, 50, 82$ , and  $126$  isotones as functions of the proton number  $Z$ . The experimental data are extracted from the  $B(E2 : 0^+ \rightarrow 2^+)$  values given in Ref. [51]. The predictions of the FRDM mass formula [36] and those of the HFBCS-1 mass formula [33] are also shown for comparison. From Fig. 4, it is easily seen that the agreement between the results of our calculations and those of the other two methods is remarkably good. All these three methods obtain essentially the same results for all the  $N = 50, 82$  and  $126$  isotones. For the  $N = 8$  isotonic chain, FRDM predicts  $^{18}_{10}\text{Ne}_8$ ,  $^{19}_{11}\text{Na}_8$ , and  $^{20}_{12}\text{Mg}_8$  to be slightly deformed, while in our calculations, these nuclei are spherical. On the contrary, the HFBCS-1 mass formula predicts all the nuclei with  $Z \geq 10$  to be slightly deformed except for  $^{24}_{16}\text{S}_8$ . For the  $N = 20$  isotonic chain, both our calculations and the FRDM method show that all the nuclei are spherical, while the HFBCS-1 mass formula predicts the nuclei with  $Z = 11, 12, 13$ , and  $25$  are deformed, which seems to be closer to the experimental data. For the  $N = 28$  isotonic chain, our calculations predict  $^{44}_{16}\text{S}_{28}$  to be deformed, which is consistent with both the experimental data and the predictions of the RHB method [52], while FRDM predicts it to be spherical. These two methods also differ in the predictions for the proton drip-line nuclei,  $^{63}_{35}\text{Br}_{28}$ ,  $^{64}_{36}\text{Kr}_{28}$ ,  $^{213}_{97}\text{Bk}_{126}$ , and  $^{214}_{98}\text{Kr}_{126}$ . We should note that these nuclei are already unstable against proton emission in our calculations (see Fig. 2). On the contrary, the HFBCS-1 method agrees with our calculations at both ends of this isotonic chain, but differs a bit in the middle: It predicts all the nuclei with  $17 \leq Z \leq 30$  to be slightly deformed. That could be the reason why there are some discrepancies between our results and those of the HFBCS-1 mass formula, as shown in Fig. 3. For the  $N = 50$  isotonic chain, the main differences between the predictions of these three methods exist in the region with  $20 < Z < 26$ . Our calculations show that these nuclei are deformed, while both FRDM and HFBCS-1 predict them to be nearly spherical.

Except for nuclei with  $Z < 18$  and  $Z > 30$  in the  $N = 28$  isotonic chain, and nuclei with  $20 < Z < 26$  in the  $N = 50$  isotonic chain, all the other nuclei in our calculations are more or less spherical. Although, at first sight, the agreement between our calculations (including the predictions of the FRDM model and the HFBCS-1 mass formula) and the experimental data is not very good, we should keep in mind the limitations of the ex-

tracting method that we obtain the experimental deformation parameters. Within such a method, even the well-known spherical nuclei,  $^{16}_8\text{O}_8$  and  $^{40}_{20}\text{Ca}_{20}$ , are predicted to be deformed [51] (see Fig. 4). Therefore, the experimental data should be compared with caution. However, combined with other experimental knowledge, such as the reduced electric transition probability,  $B(E2)$ , and  $2^+_1$  energy, we can decide whether a nucleus is really deformed. The corresponding quantities for  $^{18}_{10}\text{Ne}_8$ ,  $^{32}_{12}\text{Mg}_{20}$ , and  $^{42}_{22}\text{Ti}_{20}$  are  $0.0269(26) e^2 b^2$ ,  $1887.3(2)$  KeV;  $0.039(7) e^2 b^2$ ,  $885.5(7)$  KeV;  $0.087(25) e^2 b^2$ ,  $1554.9(8)$  KeV; respectively, which indicate these nuclei are really deformed [51]. The fact that our calculations did not find deformed ground-state configurations for these nuclei is probably due to the broken rotational symmetry in the relativistic mean field theory, which will be discussed below.

One of the long unsolved problems in the relativistic mean field theory is that it cannot obtain the deformed ground-state configurations for  $^{32}\text{Mg}$ , which is known to be strongly deformed experimentally [51], and other  $N = 20$  isotones around  $Z = 12$ , including  $^{31}\text{Na}$  and  $^{30}\text{Ne}$  [30, 53]. On the other hand, the AMD method [17], the shell-model calculations [42, 54], and the angular momentum projected generator coordinate method [55] can obtain a deformed ground-state configuration for  $^{32}\text{Mg}$ . In the shell-model calculations [42, 54], it is demonstrated that the  $2p - 2h$  intruders dominate the ground states of  $^{30}\text{Ne}$ ,  $^{31}\text{Na}$ , and  $^{32}\text{Mg}$ , therefore lead to deformed ground states for these nuclei. While the studies of the AMD method and the angular momentum projected generator coordinate method clearly show that the zero-point energy associated with the restoration of the broken rotational symmetry [56] is indispensable for a correct description of the ground state of  $^{32}\text{Mg}$ .

As mentioned above, we have performed the quadrupole constrained calculations for every nucleus in our present work in order to obtain its potential energy surface and determine the corresponding ground state. In Fig. 5, we plot the potential energy surface of  $^{32}\text{Mg}$  as a function of the deformation parameter  $\beta_2$ . For comparison, the results calculated with the parameter sets NL3 and NL-Z2 are also shown. For all the three parameter sets, an indication of a second minimum around  $\beta_2 \approx 0.5$  is clearly seen (though very “soft” for TMA and NL3), which agrees well with the unprojected AMD [17] and HFB [42] calculations. (Here it should be noted that the total energy calculated with NL-Z2 seems to deviate from those obtained with TMA and NL3 somewhat, therefore does not agree with experiment very well. It could be due to the fact that NL-Z2 is aimed at heavy and superheavy nuclei but not light nuclei like  $^{32}\text{Mg}$ . Also, we should note that TMA and NL3 adopt the same scheme of center-of-mass correction, while NL-Z2 uses the so-called microscopic center-of-mass correction [40].) Therefore, we conclude that to obtain the deformed ground-state configuration for  $^{32}\text{Mg}$ , including  $^{18}\text{Ne}$  and  $^{44}\text{Ti}$ , the broken rotational symmetry in the relativistic mean field theory has to be restored. Since so far, to our knowledge,

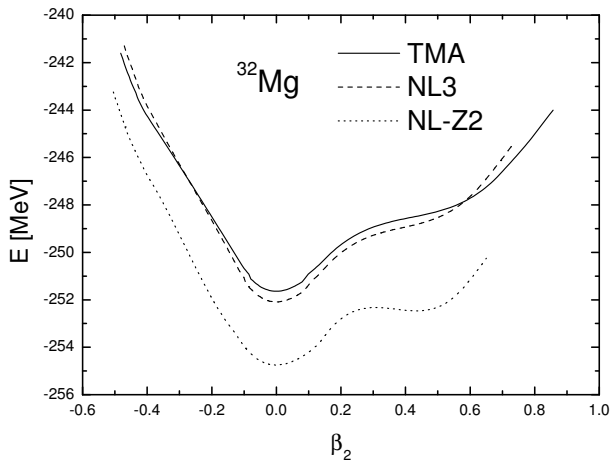


FIG. 5: The potential energy surfaces of  $^{32}\text{Mg}$  as functions of the deformation parameter,  $\beta_2$ . The solid, dashed, and dotted lines correspond to the results calculated with the parameter sets TMA, NL3, and NL-Z2, respectively.

such a calculation is still missing in the RMF method, no wonder no RMF calculations have succeeded in obtaining deformed ground-state configurations for these nuclei. We also consider this as one motivation to introduce the angular momentum projection method into the present RMF model to restore the broken rotational symmetry as one of our next works.

In Ref. [12], the authors argued that their experimental high  $Q_\beta$  value,  $8344^{+165}_{-157}$  KeV, for  $^{130}\text{Cd}$  is a direct signature of an  $N = 82$  shell quenching below  $^{132}\text{Sn}$ . While in our calculations, from the point of view of deformations, there is no indications of shell quenching for the whole  $N = 82$  isotonic chain, even in the neutron-rich side. In our calculations, the ground-state binding energy of  $^{130}\text{In}$ ,  $E = 1080.966$  MeV ( $\beta_2 = 0.041$ ), together with the binding energy of  $^{130}\text{Cd}$ ,  $E = 1072.897$  MeV ( $\beta_2 = 0.0$ ), give a  $Q_\beta$  of 8849 KeV, which falls into the category of “quenched models” defined in Ref. [12]. Therefore, whether or not the  $N = 82$  shell is quenched in the neutron-rich region needs a more careful study both experimentally and theoretically.

## VII. CONCLUSIONS

Nuclei with magic numbers are very important in the study of nuclear physics, both theoretically and experimentally. The localized feature of “magic numbers” has received more and more attention due to its importance to astrophysical problems and recent experimental developments to produce exotic nuclei in the laboratory. In the present work, we have adopted the relativistic mean

field theory to study neutron magic nuclei with six classical magic numbers  $N = 8, 20, 28, 50, 82$ , and  $126$ . The relativistic mean field theory that has proved to be very successful in describing many nuclear properties, due to its natural spin-orbit description and only a few parameters, is considered to be an ideal model to study not only stable nuclei but also exotic nuclei. In order to study all those nuclei in a proper way, we must take into account pairing correlations and deformation effects simultaneously. For nuclei with odd number of nucleons, the blocking effect must also be treated properly [57]. All these requirements make the calculation very complicated and time consuming, so up to now a systematic study in the relativistic mean field theory including all these neutron magic numbers is still missing. However, due to the importance of these nuclei to various physical problems, such a study is in urgent need. This work is also part of our series of efforts to study the magicity of magic numbers in the relativistic mean field theory.

In our systematic study of the neutron magic isotonic chains, we have found a new proton magic number  $Z = 6$  in the  $N = 8$  isotonic chain. The shell closure feature at  $Z = 14$  in the  $N = 20$  isotonic chain is also reproduced very well. We have failed, however, to obtain deformed ground-state configurations for nuclei around  $Z = 12$  in the  $N = 20$  isotonic chain, which have been attributed to the broken rotational symmetry.  $N = 28$  has been predicted to lose its magicity in the proton-deficient side of the isotonic chain, i.e. they are found to be deformed.  $N = 50$  seems to conserve its magicity in the proton-rich side while lose its magicity in the proton-deficient side. This is in agreement with its proton counterpart,  $Z = 50$ , which is also found to lose its magicity in the neutron-rich side. For the  $N = 82$  isotonic chain, we have confirmed that there is a (sub)shell closure at  $Z = 58$ , but the different deviation trends in the  $Z > 58$  and  $Z < 58$  regions seem to imply that some features are missed and/or mistreated in the relativistic mean field theory. For the  $N = 126$  isotonic chain, both the two- and one-proton separation energies are a bit overestimated. Our calculations also indicate a new (sub)shell closure at  $Z = 92$ . The binding energies agree well with experiment around  $^{208}\text{Pb}$  and become larger than experiment with increasing proton number  $Z$ . The use of two other parameter sets, NL3 and NL-Z2, does not change the above conclusion. The predicted two-proton and one-proton drip-line nuclei for the  $N = 8, 20, 28, 50, 82$ , and  $126$  isotonic chains are  $^{20}\text{Mg}_{88}$ ;  $^{46}\text{Fe}_{20}$ ;  $^{44}\text{Cr}_{20}$ ;  $^{58}\text{Zn}_{28}$ ;  $^{56}\text{Ni}_{28}$ ;  $^{100}\text{Sn}_{50}$ ;  $^{156}\text{W}_{82}$ ;  $^{152}\text{Yb}_{82}$ ;  $^{94}\text{Pu}_{126}$ ;  $^{218}\text{U}_{126}$ ; respectively.

This work was partly supported by the Major State Basic Research Development Program Under Contract Number G2000077407 and the National Natural Science Foundation of China under Grant No. 10025522, 10221003 and 10047001.

---

[1] M. G. Mayer, Phys. Rev. **75**, 1969 (1949).

[2] O. Haxel, H. H. D. Jensen, and H. E. Suess, Phys. Rev. **75**, 1766 (1949).

[3] E. M. Burbidge, G. R. Burbidge, W. A. Fowler, and F. Hoyle, Rev. Mod. Phys. **29**, 547 (1957).

[4] A. Bohr and B. Mottelson, *Nuclear structure* (New York, Benjamin, 1969).

[5] P. Ring and P. Schuck, *The Nuclear Many-Body Problem* (Springer, New York, 1980).

[6] K. Heyde, *Basic ideas and concepts in nuclear physics* (IOP, Bristol, 1999).

[7] J. D. Walecka, Ann. Phys. (N.Y.) **83**, 491 (1974).

[8] B. D. Serot and J. D. Walecka, Adv. Nucl. Phys. **16**, 1 (1986).

[9] P. G. Reinhard, Rep. Prog. Phys. **52**, 439 (1989).

[10] D. Hirata, H. Toki, T. Watabe, I. Tanihata, and B. V. Carlson, Phys. Rev. C **44**, 1467 (1991).

[11] P. Ring, Prog. Part. Nucl. Phys. **37**, 193 (1996).

[12] I. Dillmann *et al.*, Phys. Rev. Lett. **91**, 162503 (2003).

[13] A. Ozawa *et al.*, Phys. Rev. Lett. **84**, 5493 (2000).

[14] K. L. Kratz, J. P. Bitouzet, F. K. Thielemann, P. Moeller, and B. Pfeiffer, Astrophys. J. **403**, 216 (1993).

[15] R. C. Nayak, Phys. Rev. C **60**, 064305 (1999).

[16] C. Samanta and S. Adhikari, Phys. Rev. C **65**, 037301 (2002).

[17] Masaaki Kimura and Hisashi Horiuchi, Prog. Theor. Phys. **107**, 33 (2002).

[18] B. Chen, J. Dobaczewski, K.-L. Kratz, K. Langanke, B. Pfeiffer, F.-K. Thielemann, and P. Vogel, Phys. Lett. B **355**, 37 (1995).

[19] J. Meng, I. Tanihata, and S. Yamaji, Phys. Lett. B **419**, 1 (1998).

[20] L. S. Geng, H. Toki, and J. Meng, Mod. Phys. Lett. A **19**, 2171 (2004).

[21] L. S. Geng, H. Toki, S. Sugimoto, and J. Meng, Prog. Theor. Phys. **110**, 921 (2003).

[22] H. L. Yadav, S. Sugimoto, and H. Toki, Mod. Phys. Lett. A **17**, 2523 (2002).

[23] N. Sandulescu, L. S. Geng, H. Toki, and G. Hillhouse, Phys. Rev. C **68**, 054323 (2003).

[24] J. Meng, Nucl. Phys. A **635**, 3 (1998); J. Meng and P. Ring, Phys. Rev. Lett. **77**, 3963 (1996).

[25] J. Meng and P. Ring, Phys. Rev. Lett. **80**, 460 (1998).

[26] N. Sandulescu, Nguyen Van Giai, and R. J. Liotta, Phys. Rev. C **61**, 061301(R) (2000).

[27] Y. Sugahara and H. Toki, Nucl. Phys. A **579**, 557 (1994); Y. Sugahara, Ph.D. thesis, Tokyo Metropolitan University, 1995.

[28] Y. K. Gambhir, P. Ring, and A. Thimet, Ann. Phys. (N.Y.) **194**, 132 (1990).

[29] H. Flocard *et al.*, Nucl. Phys. A **203**, 433 (1973).

[30] L. S. Geng, H. Toki, A. Ozawa, and J. Meng, Nucl. Phys. A **730**, 80 (2004).

[31] J. Dobaczewski, W. Nazarewicz, T. R. Werner, J. F. Berger, C. R. Chinn, and J. Dechargé, Phys. Rev. C **53**, 2809 (1996).

[32] S. Goriely, M. Samyn, P.-H. Heenen, J. M. Pearson, and F. Tondeur, Phys. Rev. C **66**, 024326 (2002).

[33] S. Goriely, F. Tondeur, and J. M. Pearson, At. Data Nucl. Data Tables **77**, 311 (2001).

[34] M. Samyn, S. Goriely, P.-H. Heenen, J. M. Pearson, and F. Tondeur, Nucl. Phys. A **700**, 142 (2002).

[35] M. Samyn, S. Goriely, and J. M. Pearson, Nucl. Phys. A **725**, 69 (2003).

[36] P. Möller, J. R. Nix, and W. D. Meyer, At. Data Nucl. Data Tables **59**, 1 (1995).

[37] M. Bender, K. Rutz, P.-G. Reinhard, J. A. Maruhn, Eur. Phys. J. A **7**, 467 (2000).

[38] G. Audi and A. H. Wapstra, Nucl. Phys. A **595**, 409 (1995).

[39] G. A. Lalazissis, J. König, and P. Ring, Phys. Rev. C **55**, 540 (1997).

[40] M. Bender, K. Rutz, P.-G. Reinhard, J. A. Maruhn, and W. Greiner, Phys. Rev. C **60**, 034304 (1999).

[41] Z. Patyk, A. Baran, J. F. Berger, J. Dechargé, J. Dobaczewski, P. Ring, and A. Sobiczewski, Phys. Rev. C **59**, 704 (1999).

[42] E. Caurier, F. Nowacki, A. Poves, and J. Retamosa, Phys. Rev. C **58**, 2033 (1998).

[43] A. Abbas, Phys. Rev. C **29**, 1033 (1984).

[44] P. Arumugam, S. K. Patra, and A. Abbas, *arXiv:nucl-th/0309034*.

[45] K. Rutz, M. Bender, P.-G. Reinhard, J. A. Maruhn, and W. Greiner, Nucl. Phys. A **634**, 67 (1998).

[46] E. Caurier, M. Rejmund, and H. Grawe, Phys. Rev. C **67**, 054310 (2003).

[47] H. De Vries, C. W. De Jager, and C. De Vries, At. Data Nucl. Data Tables **36**, 495 (1987).

[48] F. Buchinger, J. M. Pearson, and S. Goriely, Phys. Rev. C **64**, 067303 (2001).

[49] E. G. Nadjakov, and K. P. Marinova, At Data. Nucl. Data Tables **56**, 133 (1994).

[50] I. Tanihata *et al.*, Phys. Rev. Lett. **55**, 2676 (1985).

[51] S. Raman, C.W. Nestor, JR., and P. Tikkanen, At. Data Nucl. Data Tables **78**, 1 (2001).

[52] G. A. Lalazissis, D. Vretenar, P. Ring, M. Stoitsov, and L. M. Robledo, Phys. Rev. C **60**, 014310 (1999).

[53] G. A. Lalazissis, D. Vretenar, and P. Ring, *nucl-th/0109027*; G. A. Lalazissis and S. Raman, At. Data Nucl. Data Tables **71**, 40 (1999).

[54] Yutaka Utsuno, Takaharu Otsuka, Takahiro Mizusaki, and Michio Honnma, Phys. Rev. C **60**, 054315 (1999).

[55] R. R. Rodríguez-Guzmán, J. L. Ejido, and L. M. Robledo, Phys. Rev. C **62**, 054319 (2000); Phys. Lett. B **474**, 15 (2000).

[56] P.-G. Reinhard *et al.*, Phys. Rev. C **60**, 014316 (1999).

[57] L. S. Geng, H. Toki, and J. Meng, Phys. Rev. C **68**, 061303(R) (2003).